Proceedings of ICRC 2001: 1691 © Copernicus Gesellschaft 2001

ICRC 2001

Detection of cosmic-ray antiprotons with the HEAT-pbar instrument

S. L. Nutter[1,*], A. S. Beach[1], J. J. Beatty[1], A. Bhattacharyya[2], C. R. Bower[2], S. Coutu[1], M. A. DuVernois[1,], A. W. Labrador[3], S. P. McKee[4], S. A. Minnick[1], D. Müller[3], J. A. Musser[2], M. Schubnell[4], S. P. Swordy[3], G. Tarlé[4], and A. D. Tomasch[4]**

[1]Department of Physics, The Pennsylvania State University, University Park, PA 16802, USA
[2]Department of Physics, Indiana University, Bloomington, IN 47405, USA
[3]Enrico Fermi Institute and Department of Physics, University of Chicago, Chicago, IL 60637, USA
[4]Department of Physics, University of Michigan, Ann Arbor, MI 48109-1120, USA
[*]Now at the Department of Physics and Geology, Northern Kentucky University, Highland Heights, KY 41099, USA
[**]Now at the School of Physics and Astronomy, University of Minnesota, Minneapolis, MN 55455, USA

Abstract. HEAT-pbar, a balloon instrument to measure the cosmic-ray antiproton flux from 5 to 50 GeV energy, was flown successfully in spring 2000. The instrument consists of a combination of a superconducting magnet spectrometer with time-of-flight counters and multiple wire chambers for measurements of the specific ionization. We review the instrument performance during flight and discuss how the detector configuration separates antiprotons from the large flux of electrons, muons/pions, and protons. After all data analysis cuts, approximately 70 antiprotons were detected.

1 Introduction

Heat-pbar is a balloon-borne instrument to measure the flux of cosmic-ray antiprotons with energies up to 50 GeV. Shown schematically in Fig. 1, this instrument identifies particles through the combination of a superconducting magnet, a drift tube hodoscope (DT), time-of-flight scintillators (ToF), and multiple energy loss wire chambers (dE/dx).

Previous balloon-borne cosmic-ray magnet spectrometers have used time-of-flight or Cherenkov counters to determine particle velocities. Although these techniques are successful over a certain ranges of momenta, good velocity resolution for protons in the 5 GeV/c $< p <$ 20 GeV/c region requires a different approach. The *multiple dE/dx* technique for measuring relativistic particle velocities has been used in accelerator physics experiments (Allison and Cobb, 1980), but is exploited by HEAT-pbar for the first time in a balloon-borne cosmic ray measurement. The relativistic increase in the energy loss permits a velocity measurement if the statistical fluctuations are reduced through multiple measurements. Antiprotons can be identified by mass by combining the velocity measurement with particle rigidity, determined with the magnet spectrometer, and by assuring that the particle direction is downward with the ToF. A proton event with detector hits is shown in Fig. 2.

Correspondence to: S. Nutter (scottnutter@psu.edu)

HEAT-pbar was launched by balloon from Ft. Sumner, New Mexico on June 3, 2000. The detector operated for 22 hours at an altitude between 32 and 37 km (average overburden of 7.2 g/cm^2), recording more than 1.9 million events over an integrated live time of 16.2 hours.

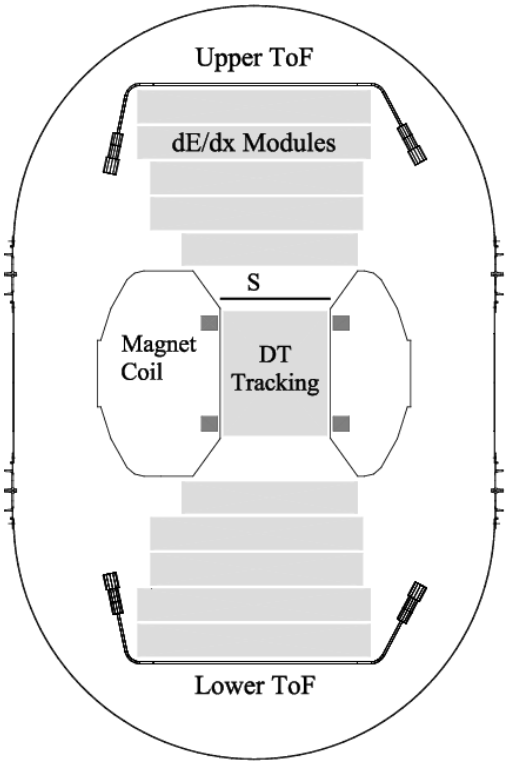

Fig. 1. Schematic diagram of the HEAT-pbar instrument. The scintillator above the DT hodoscope (S) is part of the event trigger.

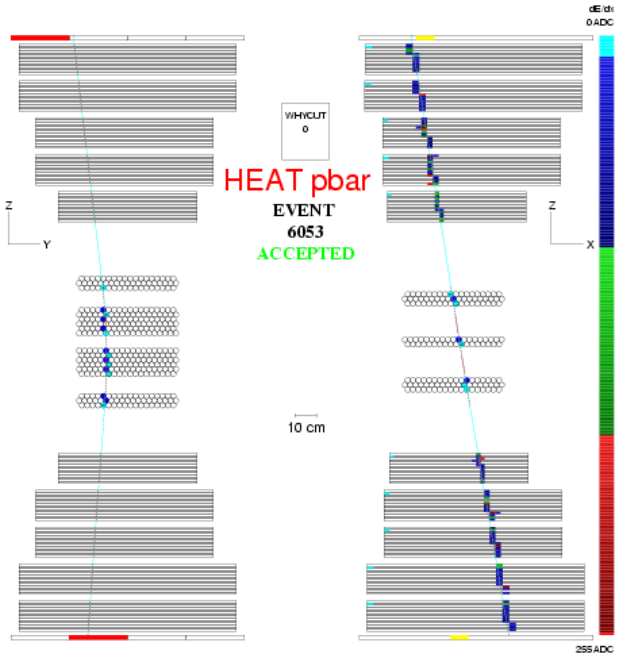

Fig. 2. A proton event shown schematically from the bending (*left*) and non-bending (*right*) directions of the DT hodoscope. Note the large number of dE/dx measurements. The different number of tube layers in the DT hodoscope between the bending and non-bending views is clearly seen. dE/dx wires are all parallel to the non-bending direction hodoscope drift tubes.

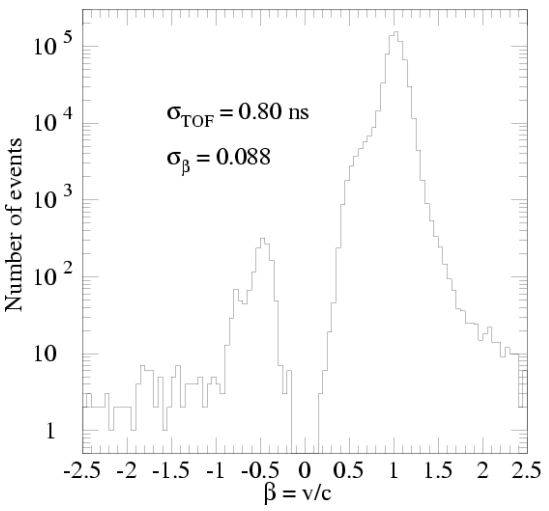

Fig. 3. Distribution in particle $\beta = v/c$ for flight events passing tracking cuts.

2 Magnet and hodoscope

A superconducting magnet with a uniform central field of 1 Tesla surrounds a hodoscope of 479 horizontally oriented 2.5 cm diameter drift tubes filled with 94% CO_2, 6% hexane gas at 1 atm pressure. Eighteen layers of tubes are oriented parallel with the magnetic field for rigidity determination (bending view), while eight layers are oriented perpendicular to the field (non-bending view). The combination of both DT views provides 3-dimensional trajectories of traversing particles. This integrated magnet and hodoscope was used previously in the HEAT-e$^\pm$ experiment and is described in detail by Barwick *et al.* (1997).

In finding a track through the DT hodoscope, an initial fit of hit DT wire centers from the bending view, and, separately, the non-bending view, is used to identify those tubes most likely to be part of the particle track. This procedure eliminates both spurious tube firings and hits due to delta rays. A DT time-to-space function is then applied to convert each recorded time to a distance of closest approach to its associated wire. For a single wire, this spatial knowledge corresponds to a circle centered on that wire. A parabolic fit to all circles initially identifies the point on each circle to be used in the next fitting step. Using the known magnetic field, these surviving points are then iteratively fit to a track with the MOMENTM routine (Wind, 1974). When completed, MOMENTM reports the rigidity (R), track fit residuals, and the maximum detectable rigidity (MDR) (Barwick *et al.*, 1997) for the candidate event.

3 Time-of-flight detector

The time-of-flight detector discriminates against upward going (albedo) particles, which can masquerade as antiprotons. In addition, ToF signals are combined with coincident hits in S (a separate layer of scintillator in the magnet bore just above the DT hodoscope) to provide a fast trigger. The ToF detector consists of two 1 m x 1 m layers of plastic scintillator separated by 2.76 m. Each scintillator layer is divided into four paddles 1cm x 25 cm x 1m in size and each end of a paddle is viewed by a photomultiplier tube (PMT). Each PMT detects approximately 40 photoelectrons for a vertical atmospheric muon traversing the center of the paddle. For a triggered event, timing and charge-integrated signal size are digitized for each participating PMT.

A histogram of $\beta = v/c$ from the flight data is shown in Figure 3. Upward- and downward-going particles are easily distinguished by the TOF detector. The standard deviation of the velocity distribution for relativistic particles is 0.088c, corresponding to a time of flight resolution of $\sim$800 ps.

4 dE/dx Measurement

The dE/dx detector system contains a total of 140 multiwire proportional chambers, each with a thickness of 1 cm, and is divided into two stacks, one above and one below the magnet. Of all fill gases, Xenon provides the strongest logarithmic rise in the energy loss curve, leading to the highest possible velocity resolution. For stable operation, 5% methane is added. Anode wires are connected in groups of 4-6 and read out by an AMPLEX (Beuville *et al.*, 1990) amplifier. Custom 8-bit ADCs digitize the amplified signals. A more

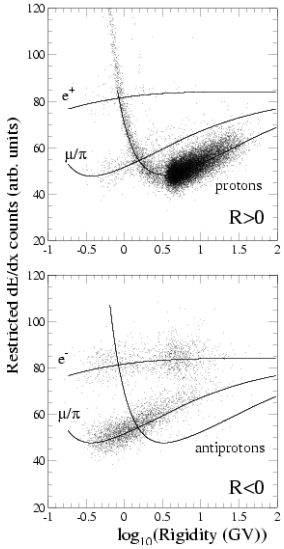

Fig. 4. *(Top)* $\langle dE/dx \rangle$ vs. $\log R$ for rigidities $R > 0$. *(Bottom)* $\langle dE/dx \rangle$ vs. $\log R$ for $R < 0$. Note the presence of the geomagnetic cutoff in the number of events at $\log 4.2\,\mathrm{GV} = 0.6$. The figures show a small fraction of the data.

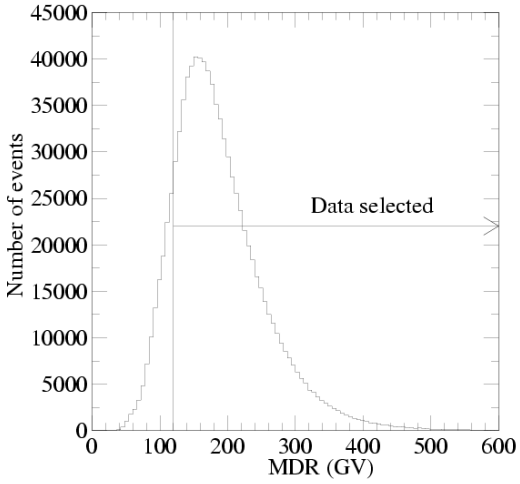

Fig. 5. Maximum detectable rigidity (MDR) distribution for flight events. Events with MDR > 120 GV were used in the analysis.

detailed description of the dE/dx system is given by Labrador *et al.* (1999).

In the analysis, only wire groups less than 5 cm from the particle track are used to build the energy loss in each MWPC layer. Signals from each retained wire group are corrected for gain variations of both the electronics and the intrinsic detector response as a function of track location in the dE/dx chambers, time during the flight, and incident angle. Corrected signals on wire groups from the same layer are summed. A restricted mean average energy loss $\langle dE/dx \rangle$ is calculated by averaging the lowest 50% of the signals of all hit layers in order to minimize the effect of Landau fluctuations.

The dE/dx system performed well during flight. The most probable number of chambers recorded in an event was 135 out of the 140 layers (>96%). The ratio of the level of relativistic proton saturation to minimum ionizing level was approximately 1.7.

5 Data Analysis

Information from the three detector systems is combined to identify particle species and kinetic energy (Fig. 4). The data were selected for good quality tracking information and consistent energy loss measurements. In the figure, note the presence of atmospheric secondaries below the magnetic rigidity cutoff at R = 4.2 GV. From Fig. 4 for negative rigidities ($R < 0$), antiprotons are seen to be rare.

Several selection criteria are applied to the ToF, DT tracking, and dE/dx information to best identify antiprotons and eliminate background. Only data taken after the instrument had reached float altitude ($\sim$33 km) are included in the analysis. Only events passing through the active scintillator region of the ToF and with $\beta > 0$ are used in the analysis. (It is possible for a particle passing through a light guide to trigger the instrument.) Tracking quality criteria require that a minimum number of drift tube layers is included in the track fit. In the bending view, at least 13 of the 18 layers must be included in the MOMENTM output, while in the non-bending view at least 6 of the 8 layers are required. In addition, we require a reasonable value for the tracking fit residual calculated from the projection of the track into the bending view. For each event, the maximum detectable rigidity (MDR) is calculated (Barwick et al. 1997). The MDR is a measure of tracking quality and field integral. We require MDR > 120 GV and $|\mathrm{MDR/R}| > 5$. For the highest rigidity range, ($25\ \mathrm{GV} < R < 50\ \mathrm{GV}$), we require $|\mathrm{MDR/R}| > 6$. The flight MDR distribution for events meeting the minimum number of DT layers hit in each view is shown in Fig. 5.

For the dE/dx data, agreement between a restricted mean energy loss calculated separately for the upper and lower sets of chambers is required. Only events in which the two values agree within two standard deviations from the mean of the difference distribution are used.

For a particular interval in particle rigidity, the antiproton to proton ratio can be determined by plotting the restricted mean energy loss distributions, identifying particle species, and determining the number of protons and antiprotons. The $\langle dE/dx \rangle$ distribution is shown for positively and negatively charged particles ($R > 0$ or $R < 0$) in Fig. 6 in the rigidity range $4.5\,\mathrm{GV} < |R| < 6\,\mathrm{GV}$. The species are easily identifiable. Gaussian fits to the data are shown. Note the extremely gaussian shape of the $\langle dE/dx \rangle$ distributions as evidenced by the high side of the electron $\langle dE/dx \rangle$ distribution (Fig. 6 *bottom*). This gaussian shape is due to the large number of samples utilized in the multiple dE/dx technique.

Antiprotons are identified as those events satisfying all se-

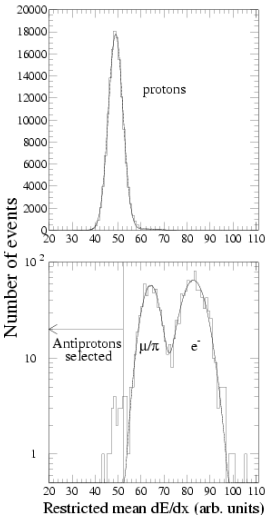

Fig. 6. Restricted mean dE/dx distribution with gaussian fits for *(top)* $4.5\ \mathrm{GV} < R < 6\ \mathrm{GV}$ and *(bottom)* $-6\ \mathrm{GV} < R < -4.5\ \mathrm{GV}$.

lection criteria and having a restricted mean energy loss of less than $P_i + \sigma_i$, where P_i and σ_i are the peak location and standard deviation of the proton distribution as determined by the gaussian fit for the i^{th} rigidity interval. Background contamination is estimated by extrapolation of the μ/π gaussian fit into the allowed antiproton region.

Antiprotons are identified in several rigidity intervals using this technique. The number of protons detected in each rigidity interval is determined by integrating the gaussian fit to the proton peak and correcting by a multiplicative factor of 0.84 to correct for counting antiproton events only up to $P + \sigma$.

6 Results

Table 1 shows the number of protons, antiprotons, and the number of estimated background μ/π events in each rigidity interval. A total of 78 antiproton candidates are identified, of which approximately 4.5 are estimated to be μ/π background events. The determination of the primary antiproton to proton abundance ratio at the top of the atmosphere is discussed by Musser *et al.* (2001).

Table 1. The number of protons and antiprotons detected in each rigidity range with estimated background to the antiprotons from pions and muons.

Rigidity (GV)	Number of protons	Number of antiprotons	Estimated μ/π background
4.5 - 6.0	119361	18	0.2
6.0 - 10	141447	23	0.4
10 - 15	60727	21	0.8
15 - 25	37742	15	0.8
25 - 50	8773	1	2.3

Acknowledgements. We thank the NSBF balloon crews that have supported the HEAT flights. This work was supported by NASA grants NAG5-5220, NAG5-5223, NAG5-5230 and NAG5-5058, and by financial assistance from our universities.

References

Allison, W. W. M. and J. H. Cobb, *Ann. Rev. Nucl. Part. Sci.*, **30**, 253-98 (1980).
Barwick, S. W. *et al.*, *Nucl. Instr. Meth. A* **400** 34-52 (1997).
Beuville *et al. Nucl. Instr. Meth. A* **288** 157 (1990).
Labrador, A. *et al., Proceedings of the 26th ICRC*, OG1.1.26, (Salt Lake City, 1999).
Musser, J. *et al., these proceedings* (2001).
Wind, H., *Nucl. Instr. Meth.*, **115** 431-434 (1974).